

X-ray spectral-timing variability of 1A 0535+262 during the 2020 giant outburst

P. Reig^{1,2}, R.C. Ma^{3,4}, L. Tao³, S. Zhang³, S. N. Zhang^{3,4}, and V. Doroshenko^{5,6}

¹ Institute of Astrophysics, Foundation for Research and Technology-Hellas, 71110 Heraklion, Crete, Greece
e-mail: pau@physics.uoc.gr

² University of Crete, Physics Department, 70013 Heraklion, Crete, Greece

³ Key Laboratory of Particle Astrophysics, IHEP, Chinese Academy of Science, Beijing 10049, China

⁴ University of Chinese Academy of Sciences, Chinese Academy of Sciences, Beijing 100049, People's Republic of China

⁵ Institut für Astronomie und Astrophysik, Kepler Center for Astro and Particle Physics, Eberhard Karls, Universität, Sand 1, D-72076 Tübingen, Germany

⁶ Space Research Institute of the Russian Academy of Sciences, Profsoyuznaya Str. 84/32, Moscow 117997, Russia

ABSTRACT

Context. The Be/X-ray binary 1A 0535+262 underwent a giant X-ray outburst in November 2020, peaking at $\sim 1 \times 10^{38}$ erg s⁻¹ (1–100 keV, 1.8 kpc), the brightest outburst recorded for this source so far. The source was monitored over two orders of magnitude in luminosity with *Insight*-HXMT, which allowed us to probe the X-ray variability in an unprecedented range of accretion rates.

Aims. Our goal is to search for patterns of correlated spectral and timing behavior that can be used to characterize the accretion states in hard X-ray transient pulsars.

Methods. We have studied the evolution of the spectral continuum emission using hardness-intensity diagrams and the aperiodic variability of the source by analyzing power density spectra. We have used phenomenological models to fit the various broad-band noise components.

Results. The hardness-intensity diagram displays three distinct branches that can be identified with different accretion regimes. The characteristic frequency of the noise components correlates with the luminosity. Our observations cover the highest end of this correlation, at luminosities not previously sampled. We have found evidence for a flattening of the correlation at those high luminosities, which might indicate that the accretion disk reached the closest distance from the neutron star surface during the peak of the outburst. We also find evidence for hysteresis in the spectral and timing parameters: at the same luminosity level, the spectrum is harder and the characteristic noise frequency larger during the rise than during the decay of the outburst.

Conclusions. As in black hole binaries and low-mass X-ray binaries, the hardness-intensity diagram represents a useful diagnostic tool to define the source state in an accreting pulsar. Our timing analysis confirms previous findings from spectral analysis of a hysteresis pattern of variability where the spectral and timing parameters adopt different values for similar luminosity depending on whether the source is on the rising or decaying phase of the outburst.

Key words. accretion, accretion disks – X-ray binaries: neutron stars – Be stars – X-ray spectra

1. Introduction

1A 0535+262 was one of the first X-ray pulsars to be discovered. The first observations date back to 13 April 1975 with the *Ariel V* mission (Rosenberg et al. 1975; Coe et al. 1975). In these first observations, the source was identified as an X-ray pulsar with a spin period of 104 s. Based on the positional coincidence with the best X-ray position, several authors (Hudec 1975; Murdin 1975) noted the V=9 mag star V725 Tau/HD245770 as a possible optical counterpart. The first suggestion of a binary system was given by Rappaport et al. (1976) by studying the variation in the 104-s periodicity. Their results were consistent with a neutron star and a OB star companion. Janot-Pacheco et al. (1987) derived a spectral type B0IIIe. Because of its high X-ray variability and optical brightness, 1A 0535+262 is one of the best studied Be/X-ray binaries (BeXB) with observations across the entire electromagnetic spectrum.

The source is not detected neither in the radio band (Tudose et al. 2010; Migliari et al. 2011) nor in the γ -ray band above $E > 0.1$ GeV (Acciari et al. 2011). Near-IR spectroscopy of the object shows that the JHK spectra are dominated by the

emission lines of hydrogen Brackett and Paschen series and HeI lines at 1.0830, 1.7002 and 2.0585 μm . Infrared excess is observed and attributed to the circumstellar disk around the Be star. The amplitudes of the JHK bands variations are about 0.1 mag on time scales of years (Persi et al. 1979; Gnedin et al. 1983; Clark et al. 1998a; Haigh et al. 1999, 2004; Naik et al. 2012; Taranova & Shenavrin 2017).

The UV observations served to estimate a mass loss rate through stellar wind from the early-type companion of $\sim 10^{-8}$ M_{\odot} yr⁻¹ and an effective temperature of 26000 K. The depth of the 2200 Å interstellar extinction feature gave a color excess of $E(B - V) = 0.72$ (Wu et al. 1983; De Loore et al. 1984; Payne & Coe 1987; Clark et al. 1998b).

1A 0535+262 displays long-term optical photometric (Hao et al. 1996; Clark et al. 1999; Lyuty & Zaitseva 2000; Zaitseva 2005) and spectroscopic (Yan et al. 2012) variability, possibly associated with mass ejection episodes as well as cyclic spectroscopic variability in the H α and other lines, which is interpreted as global one-armed oscillation in the disk (Clark et al. 1998b; Camero-Arranz et al. 2012). Asymmetric

Table 1. Log of the spectroscopic observations.

Observation	Num. of exposures	MJD (start)	Date	On-source time (s)		
				LE	ME	HE
P0304099001	1	59159.109	2020-11-06	2741	4590	4851
P0304099002	2	59161.097	2020-11-08	3253	6120	1354
P0304099003	2	59163.019	2020-11-10	3153	7170	5852
P0304099004	1	59165.074	2020-11-12	2775	4320	1725.5
P0304099005	1	59167.128	2020-11-14	1527	2850	2848.5
P0304099006	1	59169.050	2020-11-16	2702	3360	3542.0
P0304099007	1	59171.104	2020-11-18	935	1290	1412.0
P0304099008	1	59174.019	2020-11-21	899	2100	2171.0
P0304099009	1	59177.066	2020-11-21	0	360	504.0
P0304099010	1	59180.048	2020-11-21	0	600	577.5
P0304099011	1	59183.097	2020-11-30	1260	2640	1614.5
P0304099012	1	59186.015	2020-12-03	1723	3420	1157.5
P0304099013	1	59189.069	2020-12-06	3675	6720	5454.0
P0304099014	1	59191.991	2020-12-08	2280	6000	3709.0
P0304099015	1	59195.104	2020-12-12	2292	2910	1381.0
P0304099016	1	59198.018	2020-12-15	1080	3000	2160.0
P0304099017	1	59201.065	2020-12-18	1597	2160	29.0
P0304099018	1	59204.046	2020-12-21	1717	2250	0.0
P0314316001	13	59167.327	2020-11-14	20145	37267	24367
P0314316002	14	59169.249	2020-11-15	21063	37650	28733
P0314316003	20	59171.303	2020-11-18	27612	51930	37695
P0314316004	21	59174.218	2020-11-21	18535	52920	42073
P0314316005	21	59177.265	2020-11-22	25343	52380	41156
P0314316006	21	59180.247	2020-11-27	34859	51150	40294
P0314316008	20	59183.296	2020-11-30	40834	57828	46878
P0314316009	14	59186.214	2020-12-03	45422	77842	50860
P0314316010	16	59189.269	2020-12-06	31000	70950	54650
P0314316011	22	59192.190	2020-12-09	34927	58830	42155
P0314316012	20	59195.303	2020-12-12	30240	51120	34852
P0314316013	21	59198.217	2020-12-15	29576	51240	37231
P0314316014	13	59201.264	2020-12-18	25669	50940	37196

spectral lines has been associated with warped circumstellar disks during giant X-ray outbursts (Moritani et al. 2013).

In the X-ray band, 1A 0535+262 is one of the most active BeXB with frequent X-ray outbursts. 1A 0535+262 exhibits the two types of outbursts known to BeXBs (Motch et al. 1991). Regular type I outbursts show a moderate increase in X-ray flux ($L_X \lesssim 10^{37}$ erg s $^{-1}$), occur near periastron passage, and last for a fraction of the orbit. Giant or type II outbursts are significantly brighter ($L_X \gtrsim 10^{37}$ erg s $^{-1}$), do not occur at any preferential orbital phase and may last for several orbits. The November 2020 event is the fourth major outburst in the past 16 years and the brightest ever recorded.

Accreting X-ray pulsars exhibit strong X-ray variability. Periodic variability is related to the rotation of the neutron star and manifests as pulsations of the order of seconds. Another example of (Quasi) periodic variability is the type I X-ray outburst, which are orbitally modulated. The slowest time scales are linked to the mass transfer process between the Be star and the neutron star and manifest as unpredictable giant (or type II) X-ray outbursts on time scales of years. Time scales attributed to the accretion process vary in the range from fraction of a second to hours and manifest as broad-band noise in the power spectrum (Revnivtsev et al. 2009; Mushtukov et al. 2019). In addition, quasi-periodic oscillations (QPO) in the millihertz range

are commonly detected (James et al. 2010). In this work we have studied the spectral changes and the variability of the broad-band noise of 1A 0535+262 during the November 2020 X-ray outburst.

2. Observations

The source was observed by the Hard X-ray Modulation Telescope (*Insight*-HXMT, henceforth) covering the period from 6 November 2020 to 24 December 2020. *Insight*-HXMT was launched on 15th June 2017 from JiuQuan, China, runs in a low earth orbit with an altitude of 550 km and an inclination angle of 43° (Zhang et al. 2020). It carries three instruments on board: the High Energy X-ray telescope (HE) uses 18 NaI(Tl)/CsI(Na) scintillation detectors and it is sensitive to X-rays in the 20-250 keV band. It has a total geometrical area of about 5100 cm 2 and the energy resolution is 15% at 60 keV (Liu et al. 2020); the Medium Energy X-ray telescope (ME) consists of 1728 SiPIN detectors to detect photons in the 5-30 keV band using a total geometrical area of 952 cm 2 (Cao et al. 2020); the Low Energy X-ray detector (LE) contains 96 SCD detectors suitable for photons with energies in the range 1-15 keV and a geometrical area of 384 cm 2 (Chen et al. 2020). The three payloads are integrated

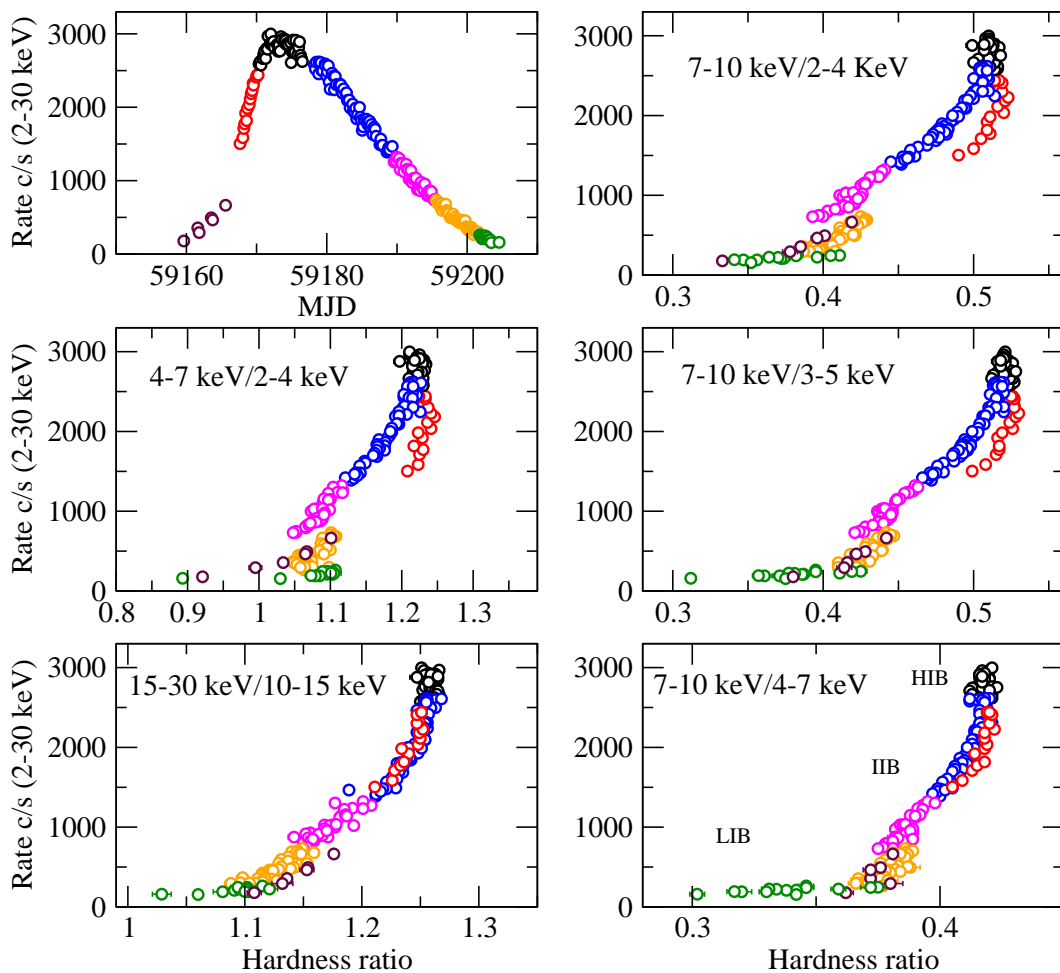


Fig. 1. Outburst light curve and hardness-intensity diagrams for various selection of the hardness ratio, shown on the top left corner of each diagram. Different colors represent different instances of the outburst as shown in the light curve (top left panel).

on the same supporting structure to achieve the same pointing direction, thus they can simultaneously observe the same source.

We analyzed observations from two different proposals: P0304099 (PI: P. Reig) and P0314316 (PI: Core Science Team). P0304099 consisted of 18 snapshots from 6 November 2020 to 21 December 2020. The observations were made every 2 days during the rise (MJD 59159–59171) and every 3 days during the decay (MJD 59171.1–59204.0). Owing to a very high count rate, no event file was generated for the *LE* instrument during the exposures P0304099009 and P0304099010. Each observation had a total duration of ~ 10 ks, although the on-source time was only a fraction of it. P0314316 covered the interval MJD 59167–59205. The observations contained multiple exposures resulting in long observing intervals. Table 1 shows the log of the HXMT observations.

The data were screened using good time intervals created with the following criteria: the Earth elevation angle greater than 10 degrees, the cutoff rigidity greater than 8 GeV, the offset angle from the pointing source less than 0.04 degrees. We also exclude the photons collected 300 s before enter and after exit the South Atlantic Anomaly.

3. Results

In this work, we focus on the general shape of the X-ray spectral continuum and the broad-band noise and their variation with X-ray luminosity. A detailed X-ray spectral analysis, including the

study of the cyclotron line was performed by Kong et al. (2021). For a detailed analysis of the millihertz quasi-periodic oscillation (QPO), see Ma et al. 2022 (in preparation).

3.1. Spectral analysis

We obtained energy spectra for each observation and each instrument. The spectra were extracted with the sole purpose to compute the X-ray flux. For this reason, we used a simple phenomenological model and fitted the spectra separately for each instrument. The continuum was fitted with a power law, modified at high energies but an exponential cutoff and at low energies by photoelectric interstellar absorption; in addition, a discrete component corresponding to the fluorescence line of iron at 6.4 keV was included in the *LE* spectral fit and a cyclotron line at ~ 45 keV in the *HE* spectral fit. These components were model with Gaussian functions in emission and absorption, respectively. To compute the X-ray luminosity, we assumed a distance to the source of 1.8 kpc (Bailer-Jones et al. 2021).

3.2. Hardness/color analysis

An X-ray color or hardness ratio is the ratio of the photon counts between two broad bands. It provides a model independent way to study the spectral changes without the need to consider com-

plex fitting procedures. On the opposite side, it depends on the detector used, hence it is instrument dependent.

To avoid possible effects of the interstellar absorption we chose energies above 2 keV. We also avoided bands containing spectral lines, e.g. 6.4 keV iron. However, for the sake of comparison with previous studies we also included the 4–7 keV band. Figure 1 shows the outburst light curve (top left panel) and the hardness-intensity diagram (HID) for various hardness ratios. The rise of the outburst was significantly faster than the decay and it is less well sampled. The source took 10–15 days to reach maximum flux, but then it took about a month to go from peak to a similar flux to the first observation. To be able to follow the motion of the source in the HID, we distinguished between the rise and the decay of the outburst and used different colors to represent various intervals that differ in the count rate. The following features may be noticed when inspecting the HID:

- Three distinct branches can be seen in the HID. At low count rate, the source moves horizontally in the HID, that is, significant spectral changes are seen for a very low change in count rate (green circles). At certain intensity, the source turns up and moves diagonally. As the intensity increases, the spectrum becomes harder. This branch contains most of the observations during the rise and decay of the outburst (brown, red, blue, magenta, and orange circles). The positive intensity-hardness ratio correlation stops near the peak of the outburst, when the source stabilizes or even moves vertically (black circles).
- The soft part of the spectrum, $E \lesssim 5$ keV, follows different tracks during the rise and decay of the outbursts. During the rise, the spectrum is harder than during the decay (compare red and blue points in Fig. 1). This hysteresis effect decreases as the energy of the bands considered increases.
- We observed a break in hardness during the decay. At ~ 700 c/s ($L_x \approx 1.7 \times 10^{37}$ erg s⁻¹ in the 2–30 keV energy range), the source jumps from the decaying track to the rising track (note the discontinuity between the magenta and the orange circles in Fig. 1). Again this effect is observed only at low energy.

3.3. Broad-band noise

The fast temporal variability of the source is characterized by periodic (pulsations) and aperiodic (red noise) components. To investigate the broad-band noise components associated with the aperiodic variability, we obtained the power spectral density (PSD) or simply power spectrum by Fourier transform of the light curves in the 30–100 keV band. We use the HE instrument because it offers the largest effective area of the three instruments. To decrease the error in each frequency bin, the light curves were divided into segments and a Fast Fourier Transform was computed for each segment (see e.g. van der Klis 1989, 2006). The final power spectrum is the average of the power spectra obtained for each segment.

The frequency interval covered by the power spectrum is given by $[1/T, \nu_{\text{nyq}}]$, where T is the duration of the segment and $\nu_{\text{nyq}} = 1/(2\delta t)$ is the Nyquist frequency. δt is the time resolution of the light curve. Because the variability of accreting X-ray pulsars at high frequencies is strongly suppressed (Reig & Nespoli 2013), most likely due to the viscous diffusion associated to accretion rate fluctuations (Mushtukov et al. 2019), the time resolution need not be too small. We set the highest frequency at 16 Hz ($\delta t = 0.03125$ s). The length of each interval was chosen to be 256 s, hence the minimum frequency is ~ 0.004 Hz. Since

our goal is to study the correlated spectral-timing behavior of the source, we obtained PSD covering the same intervals as in the color analysis. At least two PSD were obtained for each interval, except for the observations with the lowest intensity (green circles) that given the low S/N, we generated one average PSD.

To study the broad-band noise, we removed the contribution of the pulse flux from the light curves prior to the determination of the PSD (Finger et al. 1996; Revnivtsev et al. 2009). For each 1024-s segment (~ 10 spin cycles), we obtained an average pulse profile. We replicated this profile and created a light curve with the same duration and binning as the original light curve. Then we subtracted the replicated light curve from the original one. The removal of the pulse peak and its harmonics were not always satisfactory, leaving some residuals. Since we use average light curves in the 30–100 keV range, the variability of the pulse profiles with energy (Mandal & Pal 2020) may contribute to those residuals.

We tried a second method consisting of simply removing the frequency bins in the PSD most affected by the pulsations and its harmonics. The results in terms of the value of the best-fit parameters and its dependence with luminosity were consistent with the pulse removal methodology.

To fit the PSD, we followed two approaches. The first approach is that generally used in black-hole binaries. In these sources, it is common practice to describe the timing features with a function consisting multiple Lorentzians, L_i , where i determines the number of the component (Belloni et al. 2002). In 1A 0535+262, the *Insight*-HXMT PSD continuum in the 0.004–16 Hz frequency range is well described by three zero-centered Lorentzians, while another narrow Lorentzian is needed to fit the QPO. The characteristic frequency of L_i is denoted ν_{L_i} . This is the frequency where the component contributes most of its variance per logarithmic frequency interval and is defined as $\nu_L = \sqrt{(\nu_0^2 + (FWHM/2)^2)}$, where ν_0 is the centroid frequency and FWHM is the Lorentzian full-width at half maximum. For a zero-centered Lorentzian, the characteristic frequency is simply half of its width.

The second approach is to use a broken power law model. Because many accreting pulsars displays breaks in their power spectra (Revnivtsev et al. 2009; Mushtukov et al. 2019), the broken or double broken power law model has been used successfully in broad-band noise analysis (Doroshenko et al. 2014, 2020). The model parameters of a broken power law are, in addition to the normalization, the break frequency, ν_{break} and two power law indices, Γ_1, Γ_2 . A Lorentzian is added to account for the QPO.

The broken power-law fitted well the PSD of 1A 0535+262 at low luminosity (count rate below ~ 275 cs⁻¹ in 2–30 keV). Above that value or equivalently 2×10^{-8} erg cm⁻² s⁻¹ (1–100 keV), the overall rms increases and extra component is required. We tried fitting a double broken-power law model, which included a second break frequency and a third power-law index. The fit improved considerably with the reduced χ^2 changing from 2–4 to 1–2 for 65 and 62 degrees of freedom, typically. The physical meaning of the higher frequency break is not clear. It has also been observed in the super-luminous X-ray pulsar Swift J0243.6+6124, albeit at luminosities above the Eddington limit Doroshenko et al. (2020). Its frequency (~ 5 –7 Hz) is somehow higher than the frequency observed in 1A 0535+262 (1–3 Hz). However, this can be understood by the natural shift of all the frequencies that characterize the aperiodic variability of pulsars with flux and by the different magnetic field strength. Figure 2

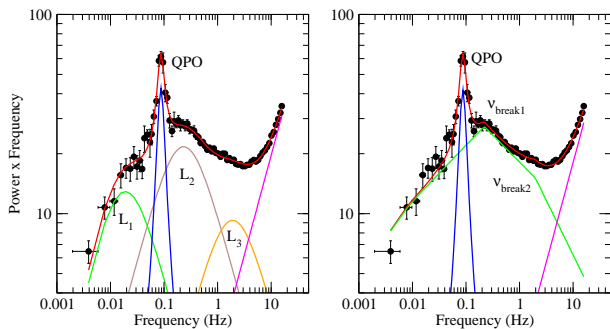


Fig. 2. Representative example of a power spectrum and model components used to fit the broad-band noise: multi-Lorentzian model (left) and broken power-law model (right). The Poisson noise was fitted with a power law with index fixed to zero (magenta line). The data correspond to observations taken during 22–25 November 2020.

shows a representative PSD and the components of the two models considered. The Poisson noise was accounted for with a power law with index fixed to zero. The two models give comparable results in terms of the quality of the fit (reduced χ^2), although the fitting parameters returned by the multi-Lorentzian model presented slightly less dispersion, especially at low luminosity. The reason may be the number of parameters involved in the fit (nine in the multi-Lorentzian model and six in the double-broken power-law model, excluding the QPO).

Figure 3 shows the dependence of the characteristic frequencies with 1–100 keV flux. The left panel displays the characteristic frequencies of the multi-Lorentzian fit, while the right upper panel shows the break frequencies of the (double) broken power law model and the QPO. The color code is the same as in Fig. 1: brown and red circles represent observations during the rise of the outburst, black points correspond to its peak, and the blue, magenta, orange, and green circles to the decay. In all cases, as the X-ray luminosity increases, the characteristic frequencies shift to higher values. The second and third power-law indices of the double broken-power law model did not change significantly during the outburst. To reduce the scatter in the frequency relation, we fixed them to their average values, $\Gamma_2 = 1.37 \pm 0.05$ and $\Gamma_3 = 1.66 \pm 0.07$. In contrast, the first power-law index, covering the lower frequency range did show a smooth decline with luminosity (lower, right panel in Fig. 3) and was left free during the fit. The QPO frequency exhibits a very tight correlation regardless of the model used. As in previous studies (Revnivtsev et al. 2009; Doroshenko et al. 2014), we find that the QPO frequency is a factor $\sim 3 - 4$ lower than the break frequency. For a detailed study of the QPO variability during the 2020 outburst, we refer the reader to Ma et al. (2022).

4. Discussion

In this work, we have investigated the changes in the spectral and timing continuum as a function of luminosity during the 2020 giant X-ray outburst of 1A 0535+262. Before we discuss our results, let us summarize the different modes of accretion in accreting pulsars.

The strong magnetic field of the neutron star in accreting X-ray pulsars disrupts the accretion flow at some distance from the neutron star surface and forces the accreted matter to funnel down on the polar caps, creating hot spots and an accretion column. The conditions prevailing in the accretion column define two accretion regimes: super- and sub-critical. These two regimes differ in the way the radiation pressure of the emitting plasma is

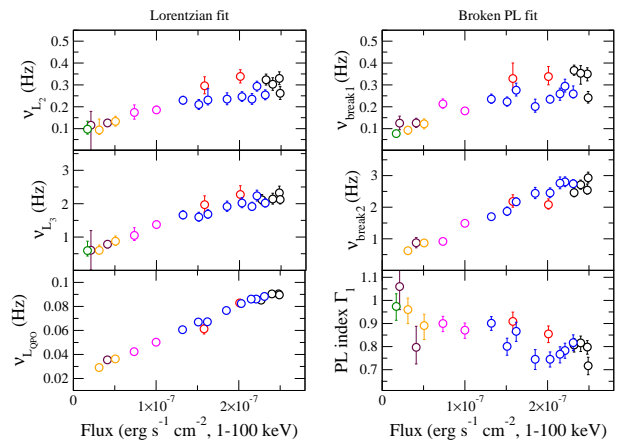


Fig. 3. Best-fit frequencies using the multi-Lorentzian model (left) and the broken power-law model (right) as a function of X-ray flux. The color code as in Fig. 1.

capable of decelerating the accretion flow. At high luminosities, in the super-critical regime, the radiation pressure dominates and the braking of the accreting matter flow is due to interaction with photons. A radiation-dominated shock stops the flow at a certain distance from the neutron star surface (Davidson & Ostriker 1973; Basko & Sunyaev 1976; Lyubarskii & Sunyaev 1982). In the sub-critical regime, the pressure of the radiation-dominated shock is not sufficient to stop the flow, which continues its way to the neutron star surface where it is decelerated by multiple Coulomb scattering with thermal electrons and nuclear collisions with atmospheric protons (Burnard et al. 1991; Harding 1994). A key parameter is the luminosity at which the source transits from the sub- to the super-critical regime. This is known as the critical luminosity, L_{crit} (Basko & Sunyaev 1976; Becker et al. 2012; Mushtukov et al. 2015).

At even lower luminosity, the Coulomb atmosphere dissipates and the matter goes all the way to the neutron star surface, possibly passing through a gas-mediated shock (Langer & Rappaport 1982). The luminosity at which this transition occurs is usually referred to as L_{coul} (see eq. (54) in Becker et al. 2012). Collisions may also result in the excitation of electrons to upper Landau levels, whose subsequent de-excitation generates cyclotron photons (Mushtukov et al. 2021). The energy spectrum at low accretion rates is characterized by two broad components that peak at $\sim 5 - 7$ keV and $\sim 30 - 50$ keV (Tsygankov et al. 2019). In the model by Mushtukov et al. (2021), the low energy hump corresponds to Comptonized thermal radiation and the high energy hump to Comptonized cyclotron photons.

Recent developments in the field have shown that this general picture should be modified at the highest luminosity. In super-Eddington X-ray pulsars (so far only Swift J0243.6+6124), a third regime has been suggested which would be associated with the transition of the inner regions of the accretion disk from the standard gas pressure dominated to the radiation pressure dominated state. This transition would occur at a luminosity one order of magnitude higher than the transition from the sub-critical to the super-critical regime (Doroshenko et al. 2020).

4.1. Hardness-intensity diagram and accretion regimes

A model independent way to study the X-ray spectral continuum is through changes in the count rate in two different energy bands (hardness ratio). The HID has proven to be a useful tool to study

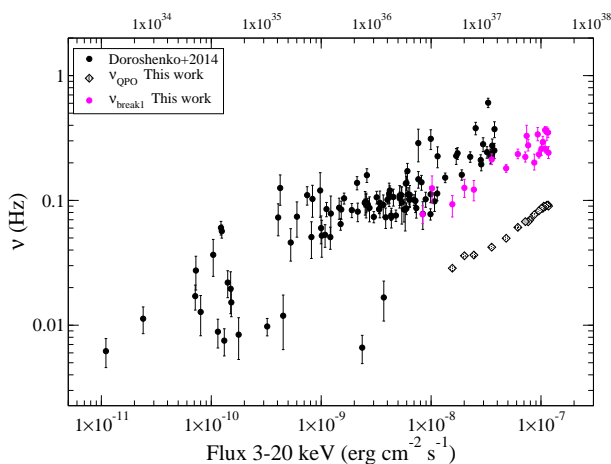


Fig. 4. Break frequencies as a function of X-ray flux. Data from *XMM-Newton*, *RXTE/PCA* (from Doroshenko et al. 2014), and *Insight-HXMT/HE*.

spectral states not only in black hole binaries and low-mass X-ray binaries (see e.g. van der Klis 2006; Belloni 2010), but also in HMXB (Reig 2008; Reig & Nespoli 2013).

Reig & Nespoli (2013) investigated the X-ray color changes during type II outbursts of nine BeXBs. They defined two main branches that were called horizontal and diagonal and that they attributed to the sub- and super-critical accretion states. Not all sources displayed the two branches. In fact, only four of the nine studied sources transitioned to a super-critical state. Reig & Nespoli (2013) concluded that in order to see a transition to the super-critical state and hence observed a clear diagonal branch in the HID the outburst peak source luminosity must be several times the critical luminosity.

Although the two branches can be clearly distinguished and identified by the direction of motion of the source in the HID — in the horizontal branch the source becomes harder as the intensity increases, whereas, in the diagonal branch the source softens as it brightens — this terminology is somehow confusing as the horizontal branch normally appears inclined when a logarithmic scale is used (confront e.g., Fig. 2 and 3 in Reig & Nespoli 2013).

In this work we shall refer to the branches by their dependency with intensity. Therefore, the almost horizontal branch at the lowest count rate (green filled circles in Fig. 1) which is formed by the first and last recorded observations of the outburst would be the low-intensity branch (LIB). The inclined branch populated by all the observations of the rise and decay at intermediate count rates would be intermediate-intensity branch (IIB). Finally, the black circles that correspond to the peak of the outburst define the high-intensity branch (HIB). The horizontal and diagonal branches in the terminology of Reig & Nespoli (2013) would be the IIB and HIB, respectively. In the case of 1A 0535+262, only the beginning of the HIB would be visible. The LIB (green circles) is reported here for the first time.

Which and how many branches appear in the HID clearly depends on the sensitivity of the detectors, the range in count rate covered by the observations and on the value of the critical luminosity. The critical luminosity is different for different sources as it strongly depends on the geometry of the accretion column and the magnetic field (Basko & Sunyaev 1976; Becker et al. 2012; Mushtukov et al. 2015). The larger the magnetic field, the higher the critical luminosity and the longer time the source spends in the sub-critical regime (IIB). Thus the reason that 1A 0535+262

does not show a well developed super-critical branch (HIB) is the high value of the critical luminosity in this system, $L_{\text{crit}} \sim 6.7 \times 10^{37} \text{ erg s}^{-1}$ (Kong et al. 2021). The maximum luminosity measured during the outburst is not significantly larger than this value. Because the ratio $L_{\text{peak}}/L_{\text{crit}}$ is not much larger than 1, the HIB (i.e. super-critical) branch does not extend toward the left and only the initial instances of this branch are observed in 1A 0535+262. Had the source luminosity increased further, we would have presumably seen the HIB extending left toward lower hardness ratio as in 4U 0115+63, EXO 2030+375, KS 1947+300 and V 0332+53 (Reig & Nespoli 2013). A transition to the super-critical regime is supported by a detailed analysis of the energy spectra, which shows sudden changes in the correlation of the photon index of the power-law component (Mandal & Pal 2020) and the cyclotron line (Kong et al. 2021) with luminosity.

The LIB (green circles in Fig. 1) is not present in any of the sources (perhaps with the exception of XTE J0658-073) studied by Reig & Nespoli (2013). Following the interpretation that the IIB and HIB correspond to the sub-critical and super-critical accretion regimes, the LIB could be associated with the transition from the Coulomb stopping to gas shock, that is, when both the radiative shock and the Coulomb atmosphere have disappeared or are too weak. The average luminosity during the LIB is $L_x \approx 6 \times 10^{36} \text{ erg s}^{-1}$, which approximately agrees with L_{coul} (Becker et al. 2012) for typical parameters of neutron stars and assuming a magnetic field of $\sim 4 \times 10^{12} \text{ G}$. At this and lower luminosity, the accretion flow is decelerated by collisions between particles. The LIB is characterized by a very fast softening of the spectrum as the count rate decreases. As the accretion rate decreases, we would expect that the collisions of the accreting particles with the electrons of the neutron star atmosphere would become less efficient. Indeed, in the framework of the Mushtukov et al. (2021) model, the relative contribution of the thermal component with respect to the cyclotron Comptonized component increases as the luminosity decreases (Tsygankov et al. 2019).

Another interesting finding is the sudden jump from the decaying track to the rising track at around 700 c/s (2-30 keV) or $2 \times 10^{37} \text{ erg s}^{-1}$ in the low energy hardness ratios (4-7/2-4 and 7-10/2-4) in Fig. 1 (transition from the magenta to the orange circles). The effect is less important at higher energy. The amplitude of change in harness ratio is 0.05 for HR=4-7/2-4, 0.02 for HR=7-10/3-5, 0.01 for HR=7-10/4-7, and non-existent for HR=15-30/10-15. It is not clear what could lead to this effect. One may argue that the count rate is not a good proxy for the accretion rate. However, the discontinuity remains even when we use luminosity or flux instead of intensity.

4.2. Broad-band noise variability

The accretion process generates strong aperiodic variability that manifest as broad-band noise in the power spectrum of BeXBs (Reig 2008; Revnivtsev et al. 2009; Tsygankov et al. 2012; Reig & Nespoli 2013; Doroshenko et al. 2014; Mushtukov et al. 2019; Doroshenko et al. 2020). The PSDs display a characteristic break that has been associated with the truncation radius of the accretion disk, at the location where the accretion disk meets the magnetosphere (Revnivtsev et al. 2009), or with the time scale of the dynamo process which is assumed to be responsible for the initial fluctuations of viscosity (Mushtukov et al. 2019) that propagate through the disk and give rise to the aperiodic variability (Lyubarskii 1997; Churazov et al. 2001).

QPOs are another prominent feature in the power spectrum of 1A 0535+262 (Finger et al. 1996; Camero-Arranz et al. 2012, see also Ma et al. 2022). Most models locate the origin of the QPO in the interplay between the accretion disk and the magnetosphere. The break frequency would be associated with the time-scales on which accretion rate fluctuations occur within the disk, while QPOs would be associated with the Keplerian time-scales at the inner edge of the accretion disk and the magnetosphere boundary. The break frequency originating in a truncated disc is expected to correlate with the Keplerian frequency at the magnetosphere.

A general property of the break and QPO frequencies is that they shift to higher values as the X-ray luminosity increases. This results is naturally explained by the relationship between mass accretion rate and the size of the magnetosphere. The magnetospheric radius scales with the mass accretion rate as $R_m \propto \dot{M}^{-2/7}$, as \dot{M} increases, the luminosity increases and the magnetosphere shrinks. The accretion disk radius decreases and the characteristic frequency at the inner edge of the disk increases. Figure 3 shows the evolution of the characteristic frequencies of the broad-band noise as a function of flux.

The large peak luminosity displayed by 1A 0535+262 during the 2020 outburst allows us to study the frequency-luminosity correlation on a broader range in X-ray luminosity as it is shown in Fig 4. This correlation initially covered two orders of magnitude in flux (Revnivtsev et al. 2009). Doroshenko et al. (2014) extended it at the lower end by analyzing observation close to quiescence. Here we extend the correlation at the higher end up to 10^{-7} erg cm $^{-2}$ s $^{-1}$. Thus, the correlation now holds for more than four orders of magnitude in X-ray flux.

Although there is large scatter in the plot, we notice a flattening of the correlation at the highest flux, already noticed in Fig. 3. In the framework of the perturbation propagation model, the break frequency observed in the PSD is related to the variability generated at the inner edge of the disk (Revnivtsev et al. 2009). Therefore, it might be that the inner parts of the accretion disk reached the closest possible distance to the neutron star at the highest luminosities.

4.3. Hysteresis

Hysteresis patterns are commonly observed in BHB (Miyamoto et al. 1995; Begelman & Armitage 2014; Weng et al. 2021) and LMXB (Muñoz-Darias et al. 2014). In this context, hysteresis means that certain spectral and timing parameters have different values depending on whether the source is in the rising phase of the outburst or in the declining phase even though the luminosity is similar. Although the number of accreting pulsars investigated is not large, some cases of hysteretic behavior have been reported. Hysteresis is not only seen in the HID (Reig 2008), but also in the pulse fraction (Wang et al. 2020) and the spin rate (Filippova et al. 2017).

In 1A 0535+262, the hysteresis pattern shows up, both in the spectral continuum and the broad-band noise. The color analysis reveals that for the same intensity, the spectral hardness is larger during the rise than during the decay of the outburst (compare the red and blue circles in Fig. 1). Also, the hysteresis pattern is most prominent at low energies. The pattern disappears as we consider higher energy bands ($E \gtrsim 4$ keV). The softer part of the spectrum of accreting pulsars is associated with thermal emission from the polar caps and/or base of the accretion column. In fact, Kong et al. (2021) found that two blackbody components were needed to fit the spectrum of 1A 0535+262 during the 2020 outburst. Interestingly, both the temperature and size

of the emitting region of the two thermal components exhibited hysteresis, with the temperatures being larger and the emitting region smaller during the rise (see Fig. 5 in Kong et al. 2021). The base of the accretion column and/or the polar cap area appear to be more compact during its formation (rise) than during its dissipation (decay). The different path during the rise and decay is also apparent in the photon index of the power-law component (Kong et al. 2021). Likewise, the characteristic frequency of the main broad-band component (ν_{Lor2} and ν_{break1}) was higher during the rise (red circles in Fig. 3). The higher frequencies may simple mean that the inner part of the accretion disk moved closer to the neutron star during the rise compared to the same luminosity during the decay.

The fact that the hysteresis is seen in both spectral and timing parameters set tight constraints on the models that seek to explain this behavior. Spectral variability occurs very close to the neutron star surface in the accretion column, while aperiodic variability originates in the accretion disk. The structure that links these two emission sites is the magnetosphere. Therefore, although there is no general consensus about the origin of the hysteresis effect in accreting pulsars, it appears to be related to a different size of the magnetosphere during the rise and decay, which would also translate into changes in the configuration of the accretion column. A smaller magnetospheric radius was also invoked to explain the higher spin-up rate in the BeXB V 0332+53 during the rise of its 2015 giant outburst (Doroshenko et al. 2017).

What causes this different size is unclear. It might be due to a variable magnetic field strength (Cusumano et al. 2016) or by a change in the emission region geometry (Poutanen et al. 2013; Doroshenko et al. 2017, but see Kylafis et al. 2021). The fact that the energy of the cyclotron line was systematically smaller during the rise (Kong et al. 2021) might indicate a weaker magnetic field. However, it is not clear how the magnetic field strength can change on such time scales. In V 0332+53, the evolution of the energy of the cyclotron line was opposite to that of 1A 0535+262, with a drop of the cyclotron line energy during the declining part. Therefore, it is difficult to think of a mechanism that would change the magnetic field strength in opposite ways for two apparently similar sources. Equally, it is not clear what could lead to the different evolution of the inner disk radius in the two sources that would favour a smaller magnetosphere during the rise in one case and a larger magnetosphere in the other source, also during the rising phase. As pointed out by Kong et al. (2021), perhaps the different spin period of the two sources, V 0332+53 is a fast pulsar ($P_{\text{spin}} = 4.4$ s), while 1A 0535+262 is a slow pulsar ($P_{\text{spin}} = 103$ s) leads to a different interplay between the accretion column and the magnetosphere. We also note that the optical counterpart to V 0332+53 is more massive (O8-9V star) and orbits at a significantly closer distance ($P_{\text{orb}} = 34$ days) than that of 1A 0535+262 (B0III star, $P_{\text{orb}} = 111$ days).

5. Conclusion

The 2020 November bright X-ray outburst of 1A 0535+262 allowed us to study the spectral-timing properties of this accreting pulsar at very high luminosity. Despite the different origin of the spectral variability (accretion column) and the broad-band noise (accretion disk), both kind of variability provide evidence for a different behavior depending on whether the source was on the rise or on the decay of the outburst. The hysteresis pattern is dominant at intermediate luminosity and low energy and appears to be related to a variable magnetospheric radius. At

similar luminosity, the inner parts of the accretion disk would move closer to the neutron star during the rise. The hardness-intensity diagram appears as a useful tool to identify accretion regimes. We observe three different branches that we identified with accretion at $L_X \gtrsim L_{\text{crit}}$ (HIB) and two branches associated with the sub-critical regime when $L_{\text{coul}} < L_X < L_{\text{crit}}$ (IIB) and when $L_X \sim L_{\text{coul}}$ (LIB). Because of its high magnetic field, the critical luminosity in 1A 0535+262 is high and the source only traces the beginning of the HIB. We have extended the correlation between the break frequency of the broad-band noise and the luminosity above $L_X > 2 \times 10^{37} \text{ erg s}^{-1}$ and now it holds over four orders of magnitude in luminosity.

Acknowledgements. ZS and TL acknowledge the supports of the National Key R&D Program of China (2021YFA0718500) and the National Natural Science Foundation of China under grant U1838201, U1838202, and 11733009. L.T. acknowledges funding support from the National Natural Science Foundation of China (NSFC) under grant No. 12122306 and the CAS Pioneer Hundred Talent Program Y8291130K2. This work has made use of the data from the Insight-HXMT mission, a project funded by China National Space Administration (CNSA) and the Chinese Academy of Sciences (CAS).

References

- Acciari, V. A., Aliu, E., Araya, M., et al. 2011, *ApJ*, 733, 96
- Bailer-Jones, C. A. L., Rybizki, J., Founesneau, M., Demleitner, M., & Andrae, R. 2021, *AJ*, 161, 147
- Basko, M. M. & Sunyaev, R. A. 1976, *MNRAS*, 175, 395
- Becker, P. A., Klochkov, D., Schönherr, G., et al. 2012, *A&A*, 544, A123
- Begelman, M. C. & Armitage, P. J. 2014, *ApJ*, 782, L18
- Belloni, T., Psaltis, D., & van der Klis, M. 2002, *ApJ*, 572, 392
- Belloni, T. M. 2010, *States and Transitions in Black Hole Binaries*, ed. T. Belloni, Vol. 794, 53
- Burnard, D. J., Arons, J., & Klein, R. I. 1991, *ApJ*, 367, 575
- Camero-Arranz, A., Finger, M. H., Wilson-Hodge, C. A., et al. 2012, *ApJ*, 754, 20
- Cao, X., Jiang, W., Meng, B., et al. 2020, *Science China Physics, Mechanics, and Astronomy*, 63, 249504
- Chen, Y., Cui, W., Li, W., et al. 2020, *Science China Physics, Mechanics, and Astronomy*, 63, 249505
- Churazov, E., Gilfanov, M., & Revnitvsev, M. 2001, *MNRAS*, 321, 759
- Clark, J. S., Lyuty, V. M., Zaitseva, G. V., et al. 1999, *MNRAS*, 302, 167
- Clark, J. S., Steele, I. A., Coe, M. J., & Roche, P. 1998a, *MNRAS*, 297, 657
- Clark, J. S., Tarasov, A. E., Steele, I. A., et al. 1998b, *MNRAS*, 294, 165
- Coe, M. J., Carpenter, G. F., Engel, A. R., & Quenby, J. J. 1975, *Nature*, 256, 630
- Cusumano, G., La Parola, V., D’Ai, A., et al. 2016, *MNRAS*, 460, L99
- Davidson, K. & Ostriker, J. P. 1973, *ApJ*, 179, 585
- De Loore, C., Giovannelli, F., van Dessel, E. L., et al. 1984, *A&A*, 141, 279
- Doroshenko, V., Santangelo, A., Doroshenko, R., et al. 2014, *A&A*, 561, A96
- Doroshenko, V., Tsygankov, S. S., Mushtukov, A. e. A., et al. 2017, *MNRAS*, 466, 2143
- Doroshenko, V., Zhang, S. N., Santangelo, A., et al. 2020, *MNRAS*, 491, 1857
- Filippova, E. V., Mereminskiy, I. A., Lutovinov, A. A., Molkov, S. V., & Tsygankov, S. S. 2017, *Astronomy Letters*, 43, 706
- Finger, M. H., Wilson, R. B., & Chakrabarty, D. 1996, *A&AS*, 120, 209
- Gnedin, I. N., Khozov, G. V., & Larionov, V. M. 1983, *Ap&SS*, 93, 207
- Haigh, N. J., Coe, M. J., & Fabregat, J. 2004, *MNRAS*, 350, 1457
- Haigh, N. J., Coe, M. J., Steele, I. A., & Fabregat, J. 1999, *MNRAS*, 310, L21
- Hao, J. X., Huang, L., & Guo, Z. H. 1996, *A&A*, 308, 499
- Harding, A. K. 1994, in *American Institute of Physics Conference Series*, Vol. 308, *The Evolution of X-ray Binaries*, ed. S. Holt & C. S. Day, 429
- Hudec, R. 1975, *Zentralinstitut fuer Astrophysik Sternwarte Sonneberg Mitteilungen ueber Veraenderliche Sterne*, 7, 29
- James, M., Paul, B., Devasia, J., & Indulekha, K. 2010, *MNRAS*, 407, 285
- Janot-Pacheco, E., Motch, C., & Mouchet, M. 1987, *A&A*, 177, 91
- Kong, L. D., Zhang, S., Ji, L., et al. 2021, *ApJ*, 917, L38
- Kylafis, N. D., Trümper, J. E., & Loudas, N. A. 2021, *arXiv e-prints*, arXiv:2108.07573
- Langer, S. H. & Rappaport, S. 1982, *ApJ*, 257, 733
- Liu, C., Zhang, Y., Li, X., et al. 2020, *Science China Physics, Mechanics, and Astronomy*, 63, 249503
- Lyubarskii, Y. E. 1997, *MNRAS*, 292, 679
- Lyubarskii, Y. E. & Sunyaev, R. A. 1982, *Soviet Astronomy Letters*, 8, 330
- Lyuty, V. M. & Zaitseva, G. V. 2000, *Astronomy Letters*, 26, 9
- Mandal, M. & Pal, S. 2020, *arXiv e-prints*, arXiv:2012.15839
- Migliari, S., Tudose, V., Miller-Jones, J. C. A., et al. 2011, *The Astronomer’s Telegram*, 3198, 1
- Miyamoto, S., Kitamoto, S., Hayashida, K., & Egoshi, W. 1995, *ApJ*, 442, L13
- Moritani, Y., Nogami, D., Okazaki, A. T., et al. 2013, *PASJ*, 65, 83
- Motch, C., Belloni, T., Buckley, D., et al. 1991, *A&A*, 246, L24
- Muñoz-Darias, T., Fender, R. P., Motta, S. E., & Belloni, T. M. 2014, *MNRAS*, 443, 3270
- Murdin, P. 1975, *IAU Circ.*, 2784, 1
- Mushtukov, A. A., Lipunova, G. V., Ingram, A., et al. 2019, *MNRAS*, 486, 4061
- Mushtukov, A. A., Suleimanov, V. F., Tsygankov, S. S., & Portegies Zwart, S. 2021, *MNRAS*, 503, 5193
- Mushtukov, A. A., Suleimanov, V. F., Tsygankov, S. S., & Poutanen, J. 2015, *MNRAS*, 447, 1847
- Naik, S., Mathew, B., Banerjee, D. P. K., Ashok, N. M., & Jaiswal, R. R. 2012, *Research in Astronomy and Astrophysics*, 12, 177
- Payne, B. J. & Coe, M. J. 1987, *MNRAS*, 225, 985
- Persi, P., Ferrari-Toniolo, M., Spada, G., et al. 1979, *MNRAS*, 187, 293
- Poutanen, J., Mushtukov, A. A., Suleimanov, V. F., et al. 2013, *ApJ*, 777, 115
- Rappaport, S., Joss, P. C., Bradt, H., Clark, G. W., & Jernigan, J. G. 1976, *ApJ*, 208, L119
- Reig, P. 2008, *A&A*, 489, 725
- Reig, P. & Nespoli, E. 2013, *A&A*, 551, A1
- Revnitvsev, M., Churazov, E., Postnov, K., & Tsygankov, S. 2009, *A&A*, 507, 1211
- Rosenberg, F. D., Eyles, C. J., Skinner, G. K., & Willmore, A. P. 1975, *Nature*, 256, 628
- Taranova, O. G. & Shenavrin, V. I. 2017, *Astronomy Reports*, 61, 983
- Tsygankov, S. S., Doroshenko, V., Mushtukov, A. e. A., et al. 2019, *MNRAS*, 487, L30
- Tsygankov, S. S., Krivonos, R. A., & Lutovinov, A. A. 2012, *MNRAS*, 421, 2407
- Tudose, V., Migliari, S., Miller-Jones, J. C. A., et al. 2010, *The Astronomer’s Telegram*, 2798, 1
- van der Klis, M. 1989, in *NATO Advanced Science Institutes (ASI) Series C*, Vol. 262, *NATO Advanced Science Institutes (ASI) Series C*, ed. H. Ögelman & E. P. J. van den Heuvel, 27
- van der Klis, M. 2006, *Rapid X-ray Variability*, ed. W. H. G. Lewin & M. van der Klis, 39–112
- Wang, P. J., Kong, L. D., Zhang, S., et al. 2020, *MNRAS*, 497, 5498
- Weng, S.-S., Cai, Z.-Y., Zhang, S.-N., et al. 2021, *ApJ*, 915, L15
- Wu, C. C., Panek, R. J., Holm, A. V., Schmitz, M., & Swank, J. H. 1983, *PASP*, 95, 391
- Yan, J., Li, H., & Liu, Q. 2012, *ApJ*, 744, 37
- Zaitseva, G. V. 2005, *Astronomy Letters*, 31, 103
- Zhang, S.-N., Li, T., Lu, F., et al. 2020, *Science China Physics, Mechanics, and Astronomy*, 63, 249502